Study of the Defect Structures in Irradiated Al- and NbC-Single Crystals by the Channeling Technique

T. Hussain, G. Linker, R. Kaufmann
J. Geerk, O. Meyer, F. Ratzel
Institut für Angewandte Kernphysik

Kernforschungszentrum Karlsruhe

COMPUTER SIMULATION OF CHANNELLING MEASUREMENTS IN CARBON-IMPLANTED NbC-SINGLE CRYSTALS

R. KAUFMANN and O. MEYER

Kernforschungszentrum Karlsruhe GmbH, Institut für Angewandte Kernphysik, P.O.B. 3640, D-7500 Karlsruhe, Federal Republic of Germany.

A Monte-Carlo-program has been used to study the channelling process in NbC-single crystals implanted with C-ions at 830°C. The dechannelling yields measured in the $\langle 110 \rangle$-direction separately for the Nb- and the C-sublattice are compared to calculated results. In the calculation two defect models (statistically displaced C-atoms and stacking faults) were applied and the characteristic parameters for these models were varied in order to reproduce the behavior of the experimental spectra. The best agreement was obtained by assuming a defect structure consisting of stacking faults with a Burger's vector of $a/6$ [$11\bar{2}$] and a stacking fault length of 7 nm. The analyzing ion beam energy was varied in the calculation and the expected energy independence of the dechannelling yield for stacking faults was found which lies in reasonable agreement with the experimental values.

1 INTRODUCTION

Refractory materials with NaCl-crystal structure such as NbC are superconductors of potential use for application. The superconducting transition temperature, T_c, of these materials strongly depends on the non-transition metal (NTM) concentration.[1] The maximum obtainable content of the NTM is often limited in an equilibrium process. For the case of NbC ion implantation has been used to increase the NTM-concentration and thus to increase T_c.[2,3] Ion implantation necessarily produces radiation damage, therefore implantation at high substrate temperatures (830°C) or implantation at room temperature followed by an annealing process up to 1200°C was necessary in order to increase T_c. Channelling measurements have been used to study the damage structure and the annealing behaviour in the Nb- and in the C-sublattice separately by determining the yields of the Nb (α,α) elastic scattering process and of the $^{12}C(d,p_0)^{13}C$ nuclear reaction.[4]

After C-implantation at 830°C a large dechannelling component up to 50% of the random level was found for the Nb-sublattice whereas for the C-sublattice the dechannelling component reached the random level. The distorted crystal was annealed at a temperature of 1070°C but the dechannelling curves were only lowered by about 5%. Therefore the crystal was annealed at 1200°C where it is known that carbon starts to diffuse. Channelling measurements showed that for both sublattices the surface region of about 300 nm was annealed. Only at greater depths the dechannelling curves were steeper than those of the unimplanted crystal.

The transition temperature T_c was 11 K right after the implantation procedure. After the first annealing process at 1070°C it was increased to 11.5 K and it was not affected by the second annealing process at 1200°C.

The experimental fact that high T_c-values are observed only for stoichiometric NbC with Nb- and C-atoms on A and B atom sites[1] seemed to be in contrast with the presence of defects which survived the first annealing stage at 900-1070°C.

A thorough analysis of this defect structure as observed by channelling measurements[4] is therefore necessary. For a compound crystal the problem arises that scattering from the A-atoms will affect the channelling parameters of the B-atom and vice versa. For a compound crystal with defects this problem is even more severe as in addition dechannelling from defects in the A-atom sublattice will influence the dechannelling from defects in the B-atom sublattice and opposite. A complicated situation like this can only be solved by computer simulation applying possible defect models. From the resulting flux distribution and

dechannelling spectra in comparison with measured spectra conclusions can be drawn on the most probable defect structure present.

In the first part the channelling parameters of an undisturbed NbC-single crystal are calculated and compared with experimental results. In the second part the influence of randomly distributed C-atoms on the flux distribution near the Nb-rows and on the dechannelling behaviour in the Nb-sublattice is calculated. In the third part results are presented which show that stacking faults are the most probable defect structure present after the first annealing stage.

2 COMPUTER SIMULATION OF THE CHANNELLING EXPERIMENTS FOR THE UNDISTURBED NbC-SINGLE CRYSTAL

A disorder analysis in damaged NbC-single crystals requires a detailed comparison of computer simulation data and measured channelling data for the undisturbed crystal. As the experiments were performed with an understoichiometric $NbC_{0.89}$ single crystal the simulation was done for a crystal with the same stoichiometry. For the structure model only C-vacancies were assumed whereas the neighbourhood of the vacancy remained undisturbed.

The special features of the Monte-Carlo-program used are described elsewhere.[5,6] For the present purpose the scattering cell was changed to the NaCl-structure type. This cell is shown in Figure 1. The atoms are assumed to vibrate isotropically and
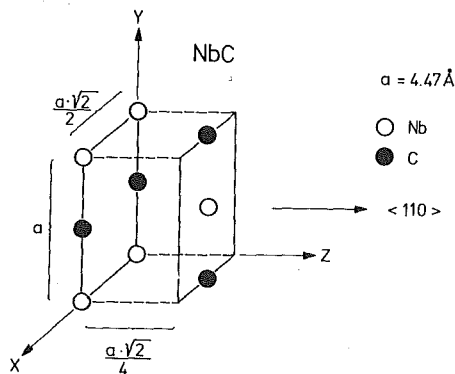
the mean vibration amplitudes have been determined from the Debye-temperatures of 390 K for the Nb- and 1100 K for the C-sublattice as evaluated from neutron scattering data.[7]

Channelling experiments have been performed with deuterons and He-ions along the $\langle 110 \rangle$-direction displaying parallel rows of Nb- and C-atoms. Normalized angular yield curves have been calculated for backscattering processes from Nb-atoms for 2 MeV-He-particles and for 1.27 MeV-deuterons. In addition the yield curves for the $^{12}C(d,p_0)^{13}C$ nuclear reaction products were calculated. These calculations have been performed for various tilt planes in order to investigate at first to what extent the critical angle, $\psi_{1/2}$, which is the half-angular width at half height between the minimum yield at a tilt angle of $\psi = 0$ deg and the random yield, depends on the tilt plane.

It has been found that the shape of the angular yield curves strongly depends on the choice of the tilt plane. Even a change of 0.5 degrees of the angle between the tilt plane and the {001} reference plane brought significant changes in the shape of the shoulders of the yield curve. The half width also varied within several hundredths of a degree. This behaviour is in agreement with experimental investigations. For this reason care was taken to use the same tilt plane in the simulation as in the experiment. Figures 2a, 2b, 2c show calculated

FIGURE 1   Scattering cell for the $\langle 110 \rangle$-channelling direction in NbC.

(a)
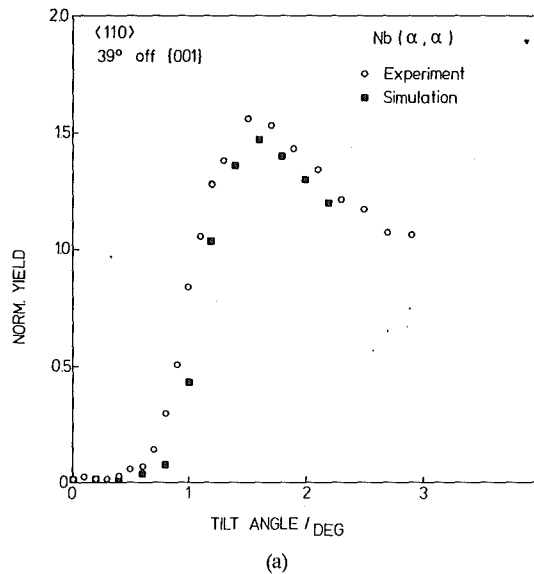
FIGURES 2a, 2b, 2c   Comparison of measured and calculated angular yield curves through the $\langle 110 \rangle$-direction for a $NbC_{0.89}$-single crystal.
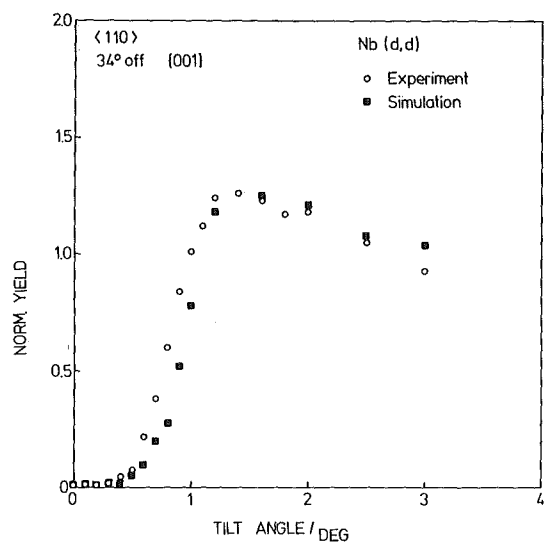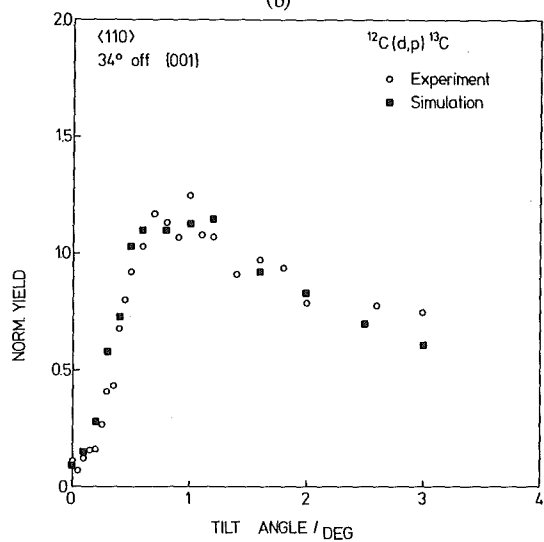
FIGURES 2b, 2c

angular yield curves in comparison to experimental results for the Nb (α,α), the Nb (d,d) and the $^{12}C(d,p_0)^{13}C$ reactions, respectively. There is good agreement in the whole shape of the yield curves, even in the formation of the significant shoulder effect. The half widths of the theoretical curves for the backscattering cases are about 0.14 degrees larger than the experimental ones whereas for the reaction case both are in agreement in the limits of the statistics. The results are presented in more details in Table I.

The difference between measured and calculated critical half angles seems to exist because of lattice distortions in the neighbourhood of C-vacancies leading to a static contribution in addition to thermal dynamic displacements. Similar lattice distortions have been observed for example in non-stoichiometric NbN.[8] The Debye temperatures used in the calculations however are derived from the phonon density distribution and take only account for the thermal part of the atomic displacements. The nature of these distortions in NbC is subject of present investigations and will not be discussed in this paper. The influence of this defect structure on the minimum yield seems to be very small as indicated by experimental χ_{min}-values of 0.015. Therefore in the following simulations the influence of these distortions on the dechannelling behaviour was neglected.

Deviations in angular yield curves can also occur due to non-ideal crystal surfaces in the experiment. Therefore in the calculation amorphous layers on the surface were simulated by choosing the transverse momentum of the starting ion from a Gaussian distribution. The thickness of the layers was determined from the surface peak area of the experimental spectra. The calculation shows that χ_{min} of the C-sublattice is more sensitive to surface layers than the χ_{min} of the Nb-sublattice. The $\psi_{1/2}$-values do not depend on layer thicknesses of 2 to 5 nm as were used in the simulation.

TABLE I

Measured and calculated χ_{min}-and $\Psi_{1/2}$-values averaged over a depth of 100 nm below the surface

Reaction	Exp. $\Psi_{1/2}$/deg	Cal. $\Psi_{1/2}$/deg	Exp. χ_{min}	Cal. χ_{min}
Nb (α,α)	0.90 ± 0.01	1.03 ± 0.01	0.015 ± 0.003	0.01 ± 0.005
Nb (d,d)	0.76 ± 0.01	0.90 ± 0.01	0.015 ± 0.005	0.01 ± 0.005
C (d,p_0)	0.34 ± 0.02	0.32 ± 0.02	0.10 ± 0.01	0.09 ± 0.01

## 3 COMPUTER SIMULATION OF THE CHANNELLING EXPERIMENTS FOR THE CARBON-IMPLANTED NbC-SINGLE CRYSTAL

$NbC_{0.89}$-single crystals were implanted at 830°C with C-ions at energies of 200 keV and 80 keV and with fluences of 1.5×10^{17} and 5×10^{16} cm^{-2}, respectively. Thus a relatively homogeneous implantation profile is achieved over a depth of 300 nm. The radiation damage was partially annealed out due to the hot implantation and T_c was about 11 K. Channelling experiments were performed prior and after implantation with 2 MeV-He-ions and 1.275 MeV-deuterons to study the damage structure in the Nb- and in the C-sublattice, respectively. After the implantation process the dechannelling yield for the C-sublattice reaches the random level whereas for the Nb-sublattice it reaches about half of the random level as can be seen in Figures 3a and 3b (solid lines No. 3). At temperatures of about 1200°C where the C-ions start to diffuse the annealing process of the damage structure is nearly completed as indicated from the dechannelling curves for both sublattices (solid lines No. 4 in Figures 3a and 3b).

3.1 Defect Model: Statistically Displaced C-Atoms

For the computer simulation two models out of the great number of possible models were chosen. Because of the 100% dechannelling yield of the C-sublattice the existence of displaced C-atoms with random distribution across the channel was assumed as a first defect structure. The depth distribution of the damage profile was chosen to be constant over a depth of 300 nm according to the implantation profile achieved by the two energies. As a free parameter the total amount of displaced C-atoms was varied until the calculated C-dechannelling yield reached the same level as determined in the experiment. The dashed lines (No. 7 and 8) in Figures 3a and 3b show the dechannelling curves for 10% and 50% displaced C-atoms, respectively. It is seen that for 50% displaced C-atoms the C-dechannelling yield reaches the random level (dashed line No. 7 in Figure 3a) whereas this large amount of displaced C-atoms does not provide any appreciable increase of the dechannelling yield for the Nb-sublattice (dashed line No. 7 in Figure 3b) in contrast to the experimental result.
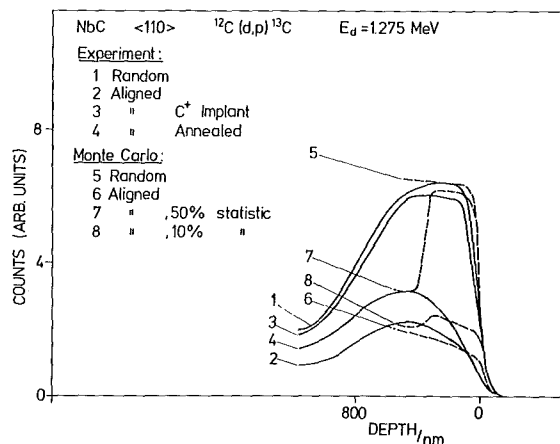
(a)
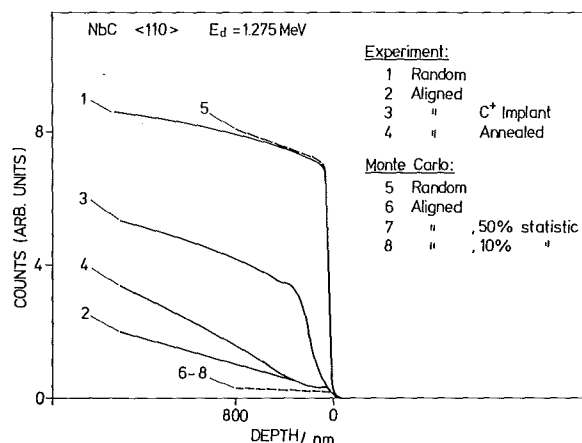
(b)

FIGURES 3a, 3b   Influence of 10% and 50% statistically displaced C-atoms on the dechannelling yield for the C-sublattice (Figure 3a) and for the Nb-sublattice (Figure 3b). Calculated spectra (dashed lines, No. 5 to 8) are compared to measured spectra (solid lines, No. 1 to 4).

3.2 Defect Model: Stacking Faults

Energy-dependent channelling measurements of the distorted NbC-crystal did not show any dependence of the dechannelling curves on the energy of incident He-particles. The same behaviour was found in analytical treatments of stacking faults by Quéré.[9] Therefore as a second defect structure a stacking fault model was inserted in the computer program using two parameters:

a) the projection of the Burger's vector onto the (110)-plane.

b) the length of the stacking fault.

From experiments on plastic deformation in refractory materials it is known that a {111} ⟨110⟩ slip system exists similar to those observed for fcc-metals.[1] In a fcc-crystal the glide motion may occur in a two step path and a perfect dislocation could degenerate into two partial dislocations (Shockley partial dislocations) thus forming a disturbed region with a stacking fault:

$$\frac{a}{2}[10\bar{1}] \rightarrow \frac{a}{6}[11\bar{2}] + \frac{a}{6}[2\bar{1}\bar{1}] + \text{stacking fault}$$

Burger's vector of a   Burger's vector of
perfect dislocation   two partial dislocations
    where a is the lattice parameter.

A similar model for the dislocation motion was proposed for refractory materials with NaCl-structure.[10] In this case the metal atoms have to move through the carbon sites and therefore it is first necessary that a carbon diffusion process occurs.

For the defect model used in the simulation a Burger's vector of $b = a/6\,[11\bar{2}]$ was used. The projection onto the xy-plane which is marked in the scattering cell in Figure 1 can be performed in two different ways described by two possible projected vectors:

$$b_x = 0; \qquad b_y = \frac{a}{6} \text{ and}$$

$$b_x = \frac{a}{6\sqrt{2}}; \qquad b_y = \frac{a}{6}.$$

The calculations have been performed for both vectors but as the results were the same only the results of simulations for the first vector of $b_x = 0$, $b_y = a/6$ are presented. As a free parameter the length of the stacking fault was varied and the results are shown in Figures 4a and 4b for the C- and the Nb-sublattice, respectively. It is seen that the dechannelling yield exhibits maxima for stacking fault lengths between 7 and 10 nm in the C-sublattice and between 5 and 7 nm in the Nb-sublattice. The depth dependence is influenced by the length of the stacking fault especially for the C-sublattice (Figure 4a). A slight rechannelling is observed beyond the damage region in the Nb-sublattice (Figure 4b).

In the channelling experiment it was found that the dechannelling yield of the C-sublattice reached random level whereas the yield for the Nb-sublattice was about 50 % of the random level. Therefore the range of the stacking fault length is limited. The experimental results are well described by choosing a Burger's vector of $b = a/6\,[11\bar{2}]$ and a stacking fault length of 10 nm. The comparison
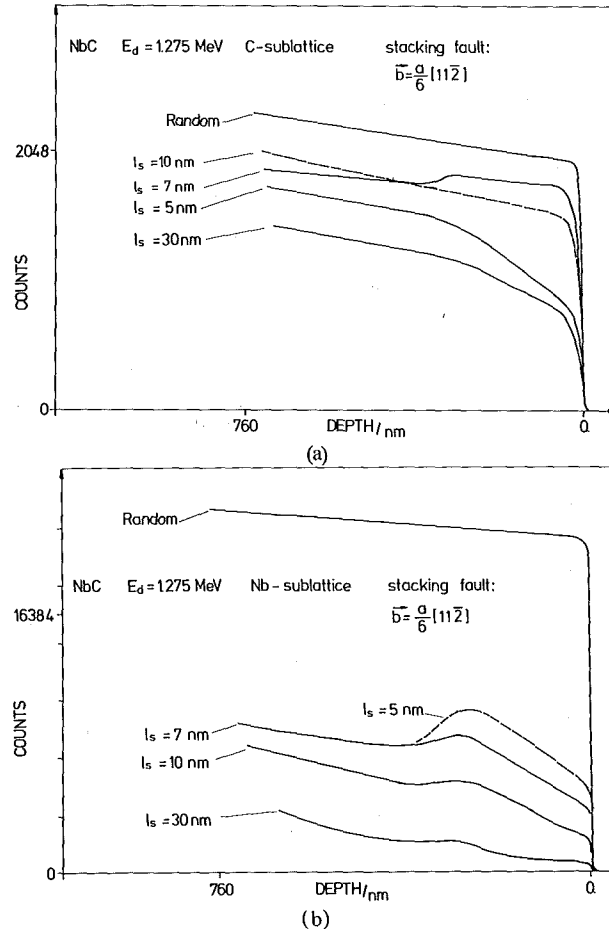
FIGURES 4a, 4b   Influence of the stacking fault length on the dechannelling yield for the C-sublattice (Figure 4a) and for the Nb-sublattice (Figure 4b). The different lengths used are indicated in the figures.

between calculated and measured values is demonstrated in the Figures 5a and 5b for the C- and the Nb-sublattice, respectively. For the C-sublattice the agreement is reasonable over the depth region considered. The deviations in the shape of the dechannelling curves are due to the energy dependence of the nuclear reaction cross section. In the simulation only a linear approximation was used which is a good fit in the surface region up to a depth of 450 nm for an incident energy of 1.275 MeV. The dechannelling behaviour for the Nb-sublattice is sufficiently reproduced in the calculation. Small differences exist in the surface region up to 200 nm. The dechannelling yield for the perfect crystal is considerably smaller than the experimental level indicating that the crystal already was slightly disturbed before implantation.
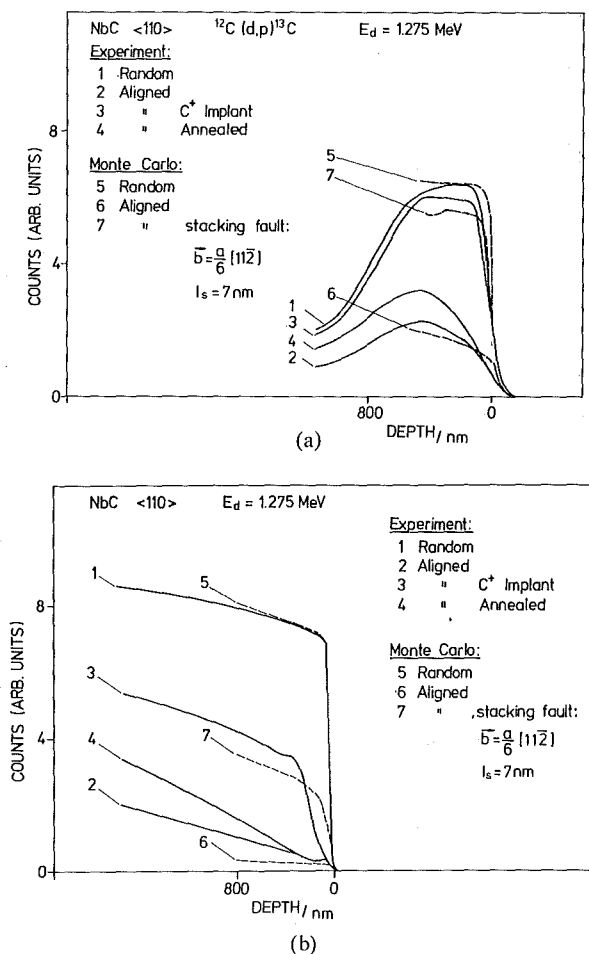
(a)

(b)

FIGURE 5a, 5b Calculated dechannelling yield with a stacking fault model of $b = a/6$ [11$\bar{2}$] and $l_s = 7$ nm in comparison with measured values.

The influence of stacking faults on the dechannelling yield for both sublattices as a function of depth can only be understood from the change of the flux distribution in the disturbed lattice. As an example the flux distributions registered along the yz-plane as indicated in the scattering cell in Figure 1 prior and after inserting stacking faults in the program are shown in Figure 6. The stacking fault parameters used were a Burger's vector of $b = a/6$ [11$\bar{2}$] and a length of 7 nm. After inserting the stacking fault the flux distribution is nearly constant between the rows whereas the amount of flux at the rows is considerably enhanced. The ratio of the flux at the C-rows to the flux at the Nb-rows explains the different dechannelling yields for the C- and the Nb-sublattices as seen in Figures 5a and 5b.
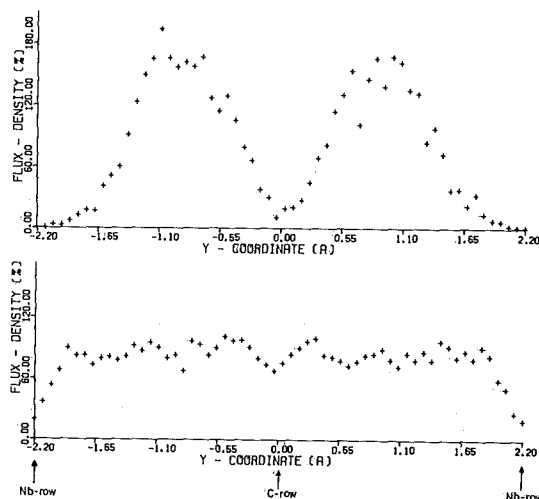

FIGURE 6   Flux distributions at a depth of 100 nm averaged over 50 nm in an undisturbed NbC-lattice (upper part) and in a lattice with stacking faults (lower part). The sectional area for the flux distributions is the yz-plane as indicated in Figure 1.

The dependence of the dechannelling yield on the analyzing beam energy provides additional information on the type of defects.[9] The dechannelling yield as a function of depth was measured for He-ions with 1.0, 2.0 and 2.8 MeV incident energy. Results of these measurements are shown in Figure 7. No energy dependence could be observed up to a depth of 250 nm. This fact excludes point defects. The calculated values do not show any energy dependence in the limits of statistical errors thus confirming the analytical
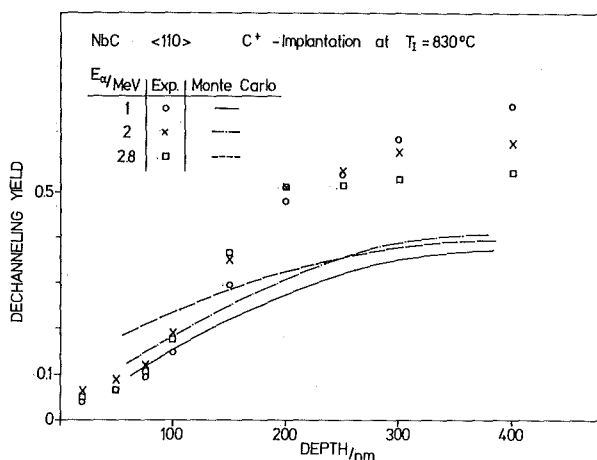

FIGURE 7   Depth dependences of measured and calculated dechannelling yields for He-ions of 1, 2 and 2.8 MeV incident energy, scattered from Nb-atoms.

treatment of stacking faults by Quéré.[9] Nevertheless, there are differences in the height of the dechannelling curves between measured and calculated values indicating that the simulation model is not yet optimized.

4 DISCUSSION AND CONCLUSIONS

The superconducting transition temperature of 11 K in NbC-single crystals implanted with C-ions at 830°C can be understood by assuming that all atoms occupy their lattice sites and that the C-vacancies are filled with C-atoms after implantation. This seems to be in contrast to the dechannelling behaviour of the C-sublattice proposing a statistical distribution of C-atoms or the formation of C-precipitates. The answer to this apparent contradiction could be ruled out by the computer simulation using statistically displaced C-atoms as a defect model. The calculated spectra for the C-sublattice showed a strong rechannelling behind the disordered C-layer in contrast to measured spectra. The calculation further revealed that the disordered C-sublattice does not affect the dechannelling behaviour in the Nb-sublattice. Thus the measured dechannelling yield from the Nb-sublattice must be attributed to damage in the Nb-sublattice. The fact that the dechannelling yield in the Nb-sublattice does not depend on the analyzing beam energy already rules out the existence of high dislocation densities and suggests the defect model of stacking faults.[9]

Stacking faults have been observed in refractory materials[1] and mechanisms for glide motion similar to those found for fcc-metals have been proposed.[10] The observed annealing behaviour of the damage in implanted NbC above 1200°C at temperatures where the C-atoms start to diffuse can well be explained by annealing of stacking faults due to glide motion.

For the defect model only one parameter namely the length of the stacking fault has been used

because the Burger's vector in refractory materials is known, $\mathbf{b} = a/b$ [$11\bar{2}$]. By choosing a length of 7 nm the measured dechannelling yields could reasonably be reproduced in the simulation. The difference in the flux distribution near the Nb- and the C-rows for such a defect model provides an explanation for the higher dechannelling yield for the C-sublattice in comparison to the observed yield for the Nb-sublattice. The calculated dechannelling yield does not show any energy dependence. This confirms the result of an analytical treatment of stacking faults by Quéré.[9] As in principle all atoms remain on regular lattice sites this model also seems to explain the measured high T_c-value.

The restrictions of the defect model used in the simulation are obvious as the agreement between theoretical and experimental results is not perfect. This fact indicates that the model has to be improved in details. Nevertheless, this defect model gives qualitative agreement which is good enough to solve the contradiction between high T_c and high C-dechannelling yield in C-implanted NbC-single crystals.

REFERENCES

1. A summary is given by L. E. Toth: *Refractory Materials*, Vol. 7, Academic Press (1971).
2. J. Geerk and K. G. Langguth, *Solid State Comm.*, **23**, 83 (1977).
3. J. Geerk, K. G. Langguth, G. Linker, and O. Meyer, *IEEE Trans. on Mag. MAG-13*, 662 (1977).
4. J. M. Lombaard and O. Meyer, *Rad. Eff.*, **36**, 83 (1978).
5. H. D. Carstanjen and R. Sizmann, *Rad. Eff.*, **12**, 225 (1972).
6. R. Kaufmann and O. Meyer, *Rad. Eff.*, **40**, 97 and 161 (1979).
7. F. Gompf, L. Pintschovius, W. Reichard, and B. Scheerer, *Proc. Conf. on Neutron Scattering, Gatlinburg*, June 1976, Vol. 1, p. 129.
8. M. Müllner, W. Reichardt, A. N. Christensen, Progress Report of the Teilinstitut Nukleare Festkörperphysik, Kernforschungszentrum Karlsruhe, KFK **2881**, 5 (1979).
9. Y. Quéré, *Rad. Eff.*, **28**, 253 (1976).
10. D. J. Rowcliffe, Ph.D. Thesis, University of Cambridge, (1965).

RADIATION DISORDER AND LATTICE LOCATION IN ION IMPLANTED ALUMINIUM CRYSTALS

T. HUSSAIN† and G. LINKER

Kernforschungszentrum Karlsruhe, Institut für Angewandte Kernphysik I, 7500 Karlsruhe, Postfach 3640, Federal Republic of Germany

Aluminium single crystals have been implanted with S, Ca, Cu, Ga, Ge and Cs ions with energies corresponding to similar projected ranges. Energy dependent channelling and Rutherford backscattering experiments have been performed in the energy range of 1–3 MeV using $^4He^+$ ions as the analyzing particles. The aligned spectra of Cu, Ga, Ge and Cs implanted samples showed a monotonous increment of the dechannelling yields with depths and no disorder peaks have been observed. The dechannelling yields determined from these spectra revealed a $\sqrt{E}$ dependence with a relatively higher slope for the Cs implanted sample compared to the others. The Ge implanted sample showed very little dependence on $\sqrt{E}$. However, the spectra of the S and Ca implanted samples showed disorder peaks within approximately the measured projected range as the energy of the analyzing beam was increased. The lattice positions of these ions in Al are also reported. S, Ca, Cs and Ge showed no or little substitutional occupation, however, Cu and Ga showed high (>70 %) substitutionality but the atoms were displaced some tenths of an angstrom from the ideal lattice site.

INTRODUCTION

Combining the use of the channelling effect and Rutherford backscattering (RBS) experiments, defect analyses in ion-implanted semiconductors and in metal single crystals have been carried out by many groups, e.g.[1–5] In the aligned spectra of ion implanted semiconductors a direct backscattering peak (generally called disorder peak) is normally observed within the ions projected range. The backscattering peak is a result of localized disordered atomic configurations, where each atom acts as an individual scattering center. Since the channelled ion has a high probability to interact with the atoms which are displaced from the ideal lattice position to a distance of greater than the Thomas–Fermi screening radius (i.e. >0.1–0.2 Å), the direct scattering peak may be observed in the aligned spectra depending on the distribution of the displaced atoms.

In ion implanted metals, normally the disorder peak is not observed. For small displacements from the lattice position the direct scattering contribution becomes negligible compared to the dechannel-

ling yield. This dechannelling yield arises from extended defects like dislocations, interstitial clusters or bubbles with associated strains. The curvature of the atomic rows and planes in the neighbourhood of such defects may alter the trajectory of channelled particles and hence produce dechannelling.

With the help of transmission electron microscopy (TEM) one can correlate the dechannelling behaviour with damage configurations in metals. If this is not done, then according to the suggestions given by Quéré,[6] the energy dependence of the dechannelling cross-sections may give information about the nature of defects. As suggested by him the dechannelling yields from channelling backscattering experiments depending on analyzing beam energy like $E^{1/2}$ would indicate a contribution of dislocations,[7] a E^0 dependence—stacking faults, gas bubbles or cavities[8] and a $E^{-1/2}$ dependence—interstitial atoms.[9] Considering the energy dependence of dechannelling cross-sections as a diagnostic tool, defect analyses on ion implanted single crystals have been performed by some workers, e.g.[10–14]

Here we present results from energy dependent dechannelling analyses of S, Ca, Cu, Ga, Ge and Cs implanted aluminium crystals together with their lattice positions. Besides the general interest of

† On leave from Physics Department, University of Dacca, Bangladesh.

disorder analyses with channelling effect measurements, the problem arose from previous experiments on the change of the superconducting transition temperature T_c of implanted aluminium layers. In these experiments different changes of T_c occurred depending on the implanted ion species. Rather large T_c increases ($\Delta T_c \geq 0.5$ K) were observed for ions like N, S, Ca or Cs while smaller or no effects ($T_c \leq 0.2$ K) were observed for Cu, Zn, Ga, Ge or Ag ions.[15] The question was whether the T_c changes are due to an alloying effect or rather to distortions of the Al host lattice. Some results for Ca and Ga implantations have already been reported.[16]

EXPERIMENTAL

An aluminium $\langle 100 \rangle$ oriented single crystal rod was purchased from Materials Research Corporation, New York, and was cut into slices with an acid wire saw device using a solution of HCl and H_2O (1:1 proportion by volume). The slices were carefully lapped using successively 7–1 μ diamond pastes and after annealing at 500°C for 2 hours under a vacuum of $\sim 10^{-6}$ Torr, electropolished in a 1:1 solution of CH_3OH and HNO_3. The samples were checked by ion-channelling and backscattering measurements showing a minimum yield of 5–6% along the $\langle 100 \rangle$ direction determined behind the surface peak. The spectra of the aligned crystals showed only a small increase of the dechannelling rate with depths indicating a low density of defects. The samples were then implanted at room temperature along a nonchannelling direction. The implantation parameters are summarized in Table I.

The analyses of the implanted samples were performed with a well collimated $^4He^+$ beam obtained from a Van-de-Graaff accelerator in the energy range of 1–3 MeV using channelling and Rutherford backscattering. The beam current was 15–20 nA. The particles backscattered at an angle of 165° were detected by a solid state surface barrier detector with an energy resolution of 15 keV and with standard electronics including a pulse pile-up rejection system. The alignment of the crystals was performed on a three-axis electronically controlled goniometer capable of rotation at steps of 0.01°. The samples were rotated around an axis well off the channelling direction for detection of the random spectra.

RESULTS

a) Energy Dependent Measurements

As examples, Figures 1 and 2 show $\langle 100 \rangle$ aligned backscattering spectra of Cu and Cs implanted aluminium crystals at different energies of the analyzing $^4He^+$ beam. No disorder peaks are observed in the spectra, however, an increase of the dechannelling yields as a function of depth is noticed with characteristic "knees" giving maximum disorder depth. These "knees" are well observed at higher analyzing beam energies. The average disorder depth X_D, defined as the distance between the "knee" and the sample surface, was found to exceed the measured ions projected range distribution. Random stopping cross-sections from Ziegler and Chu[17] have been used for the conversion of energy to depth scale. In Table I, the implantation parameters, LSS range, measured range and disorder depth are summarized for all ions used in these experiments.

According to the analysis of Merkle et al.,[18] the average defect dechannelling cross-section

TABLE I

Implantation parameters: energy, fluence and LSS range R_p, measured range and disorder depth X_D

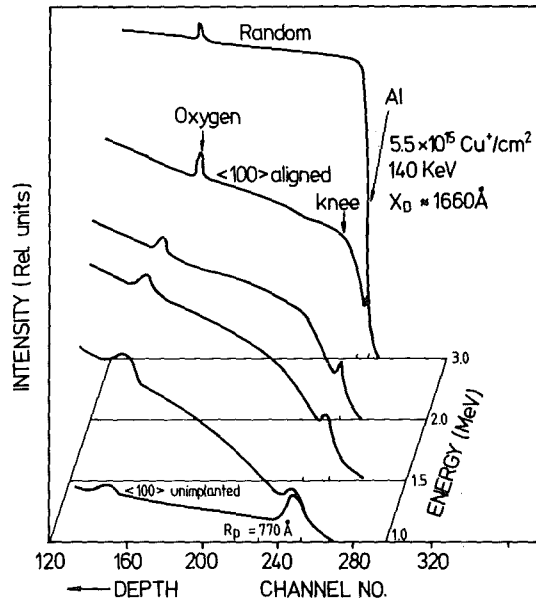| Ion	Implantation energy (keV)	Fluence ions/cm^2	LSS Range R_p (Å)	Measured Range (Å)	Disorder depth X_D (Å)
S	80	3.5×10^{16}	810	930	1060
Ca	90	1.5×10^{16}	820	1000	1110
Cu	140	5.5×10^{15}	770	1100	1660
Ga	150	7.0×10^{15}	780	1100	2150
Ge	150	5.1×10^{15}	760	1100	2000
Cs	220	3.4×10^{15}	740	800	1300

FIGURE 1 Backscattering spectra of a $\langle 100 \rangle$ aligned Al crystal implanted with 5.5×10^{15} Cu$^+$/cm^2, 140 keV, at four different analyzing beam energies. A random and an aligned spectrum for an unimplanted crystal are also shown. Different depth scales in the spectra are indicated by the ions projected range R_p.
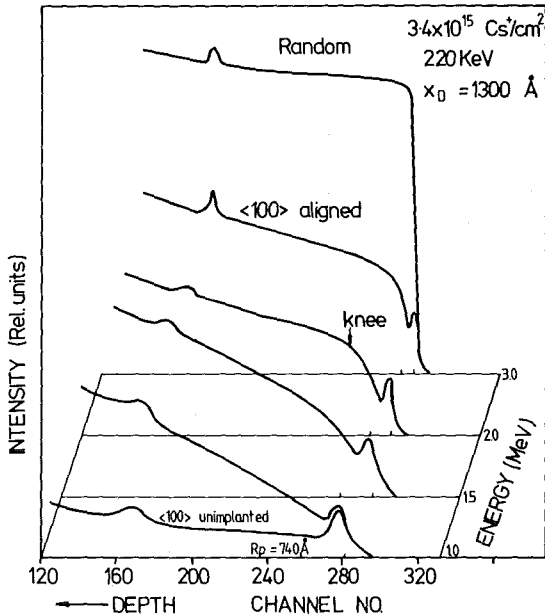

FIGURE 2 Backscattering spectra at different analyzing beam energies of a $\langle 100 \rangle$ aligned Al crystal implanted with 3.4×10^{15} Cs$^+$/cm^2, 220 keV.

from defect clusters in ion bombarded crystals can be determined by using the formula

$$\sigma_d = \frac{1}{N_s} \Delta\left(\frac{\partial \chi}{\partial z}\right) \frac{1}{1 - \chi_{min}} \qquad (1)$$

where N_s is the defect density, $\Delta(\partial\chi/\partial z)$ is the damage induced change of the dechannelling rate and χ_{min} is the minimum yield. The value of $\Delta(\partial\chi/\partial z)$ here is obtained from the slope of the line fitting data points in the spectrum where the maximum disorder is present. This procedure has been adopted because of the low increase of the dechannelling rate in the unimplanted crystals. The minimum yield χ_{min} is found by extrapolating the fitting lines to the surface. Using Eq. (1), the product $\sigma_d N_s$ is determined for the different analyzing beam energies and is shown in Figure 3(a, b, c) in a plot versus $\sqrt{E}$ for Cs, Ge and Cu implanted samples. These figures show the variation of σ_d with the beam energy directly since N_s is constant (independent of energy) for a particular sample. Straight lines passing through the experimental data points verify a $\sqrt{E}$ dependence of the dechannelling cross-section. Different slopes were observed for the various implanted ion species with the largest slope occurring for Cs while much lower slopes were observed in a decreasing order for Cu, Ga and Ge, respectively. The above results were compared with a similar type of analysis using the formula $-\ln[(1 - \chi_D(z))/(1 - \chi_V(z))]$ of Piraux et al.[19] This expression, where $\chi_D(z)$ is the ratio of aligned to random yields in case of the implanted sample at a depth z where maximum disorder is present and $\chi_V(z)$ is the same ratio in case of the vigin crystal, is proportional to the dechannelling cross-section. A similar dependence on $\sqrt{E}$ was found as in the results presented above.

Figure 4 shows the $\langle 100 \rangle$ aligned backscattering spectra from a S implanted sample. Here one observes a disorder peak at a depth slightly deeper than the measured ion range distribution. At 1 MeV the disorder peak could not be resolved. This type of disorder peak was also observed in Ca-implanted Al,[16] Co implanted Al[20] and N implanted Al.[12] Disorder peaks have also been observed in N implanted vanadium and C implanted molybdenum single crystals.[10] The appearance of such peaks in metals is an exceptional case.

Due to the appearance of disorder peaks, here a different procedure for the analysis of the energy dependence of the dechannelling yield has been
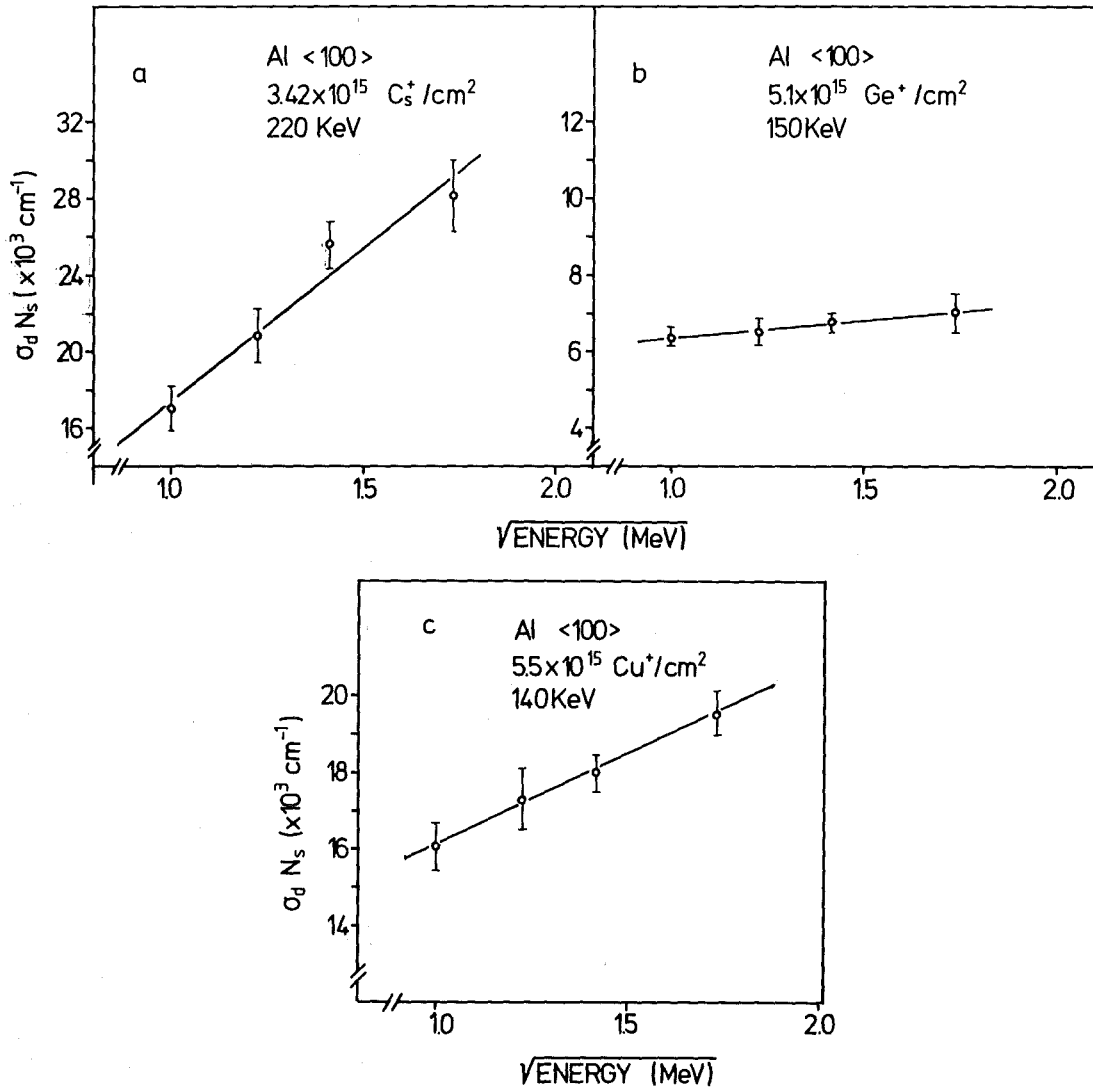
FIGURE 3 Dependence of $\sigma_d N_s$ on the square root of the analyzing beam energies of $\langle 100 \rangle$ aligned Al crystals implanted with (a) Cs, (b) Ge and (c) Cu ions as indicated in the figure.

used. Figure 5 shows this dechannelling yield $\Delta\chi$, namely, the difference of the dechannelling yields of the implanted and the virgin crystal, determined at a depth behind the disorder peak as a function of the analyzing energy. The observed slight decrease of $\Delta\chi$ with increasing energy is in accordance with the dechannelling behaviour from that part of disorder which gives rise to a direct backscattering peak. Similar slight decreases of $\Delta\chi$ with energy have been observed in our previous measurements in Ca implanted Al single crystals[16] and in N implanted vanadium

and C implanted molybdenum[10] with similar high intersection values of the straight lines fitted to the experimental points on the $\Delta\chi$-axis.

b) Lattice Occupancy

The lattice occupany of the implanted ions was measured by comparing the random and aligned backscattering yields of the impurity atoms and in some cases complete angular scans were also performed. The $\langle 100 \rangle$ aligned and random backscattering yields for the ions like S and Cs were
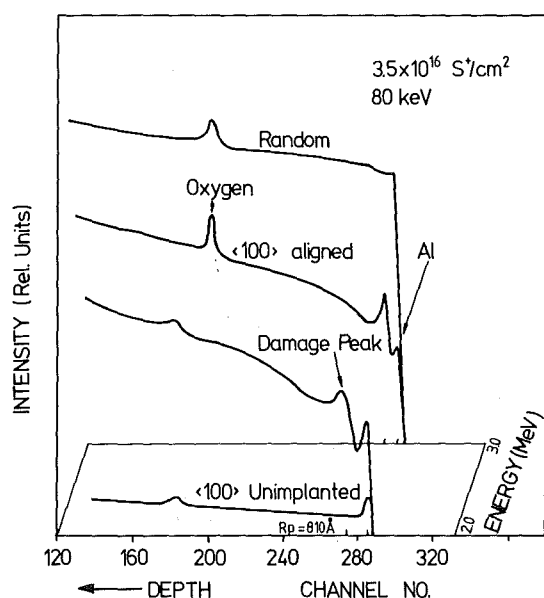
FIGURE 4 Backscattering spectra at two different energies of a $\langle 100 \rangle$ aligned Al crystal implanted with 3.5×10^{16} S$^+$/cm^2, 80 keV.
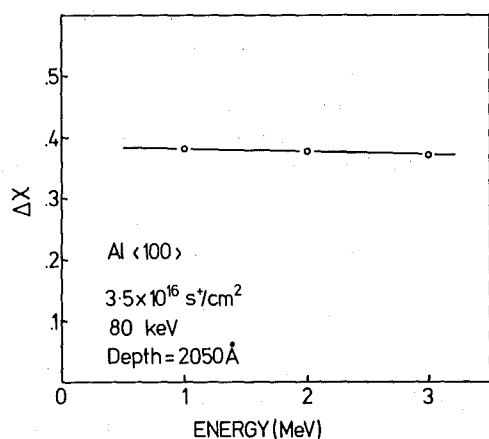

FIGURE 5 Dechannelling yield $\Delta\chi$ from a S implanted Al crystal as a function of analyzing beam energies. $\Delta\chi$ was determined at a depth of 2050 Å (behind the damage peak).

found to be almost the same, i.e. these ions have no tendency for occupying lattice sites. Figure 6 shows spectra from a Ge implanted Al crystal at 2 MeV ^{4}He$^+$ beam. The Ge yields for aligned and random directions show that about 30% of the Ge atoms occupy lattice sites as estimated along the $\langle 100 \rangle$ direction. The Cu yield indicated that a larger fraction of Cu atoms occupied substitutional lattice sites. In this case angular scans were per-
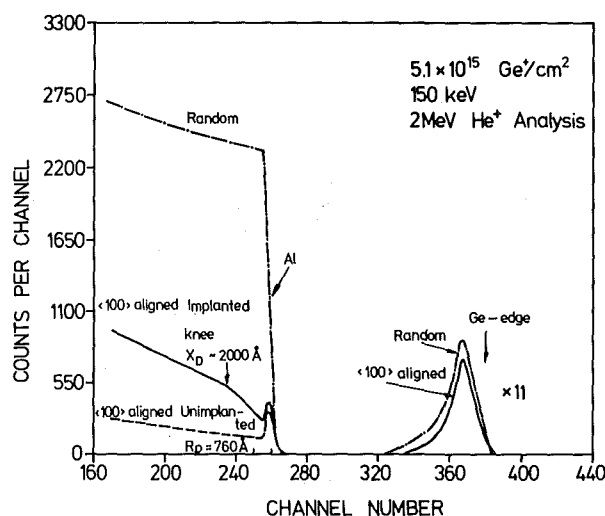

FIGURE 6 Random and $\langle 100 \rangle$ aligned backscattering spectra from a Ge implanted Al crystal at 2.0 MeV ^{4}He$^+$ beam.

formed. Since in crystals with fcc structure a 17% shadowing for atoms well displaced (0.5–1.5 Å) into $\langle 110 \rangle$ directions occurs when channelling experiments are performed along the $\langle 110 \rangle$ direction[21] additional angular scans were performed along the $\langle 100 \rangle$ direction to obtain an unambiguous lattice site determination. Figure 7(a, b) show the angular scans of the backscattering ^{4}He yields across $\langle 100 \rangle$ and $\langle 110 \rangle$ channels from a Cu implanted Al crystal at an incident beam energy of 2 MeV He$^+$. The energy windows were set at a depth equivalent to the Cu ions range for both host and impurity. The substitutional fraction for Cu in Al was calculated by using the formula $f_s = (1 - \chi_i)/(1 - \chi_h)$,[22] where χ_i and χ_h are the normalized minimum yields for impurity and host respectively. About 73% of Cu is found to occupy substitutional sites.

In the angular scans for Cu it is seen that the angular width is narrower than for the host. A similar narrowing effect has also been observed in a Ga implanted sample which showed 87% substitutionality.[16] Figure 8 shows an angular scan along $\langle 100 \rangle$ from a Ga implanted (5.3×10^{15} Ga/cm^2, 150 keV) Al sample at 3 MeV He$^+$. The narrowing of the impurity signal half width is an indication that the Cu or Ga atoms are displaced from the ideal lattice sites. The distribution of the displacements from the lattice sites can be simulated by increasing the rms vibrational amplitude. The average displacements of Cu or Ga from the Al lattice along the $\langle 100 \rangle$ direction have been
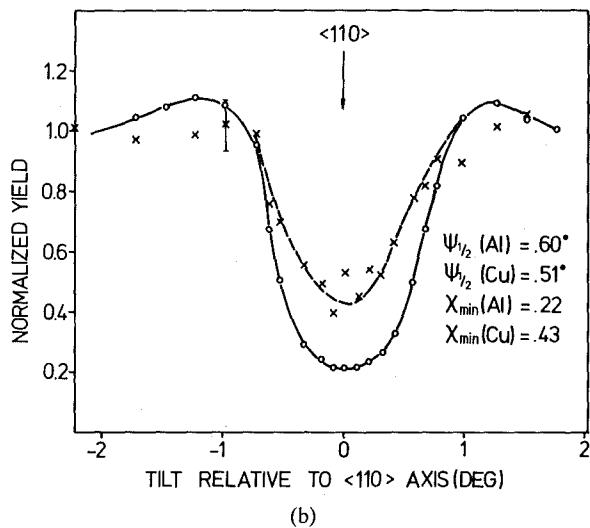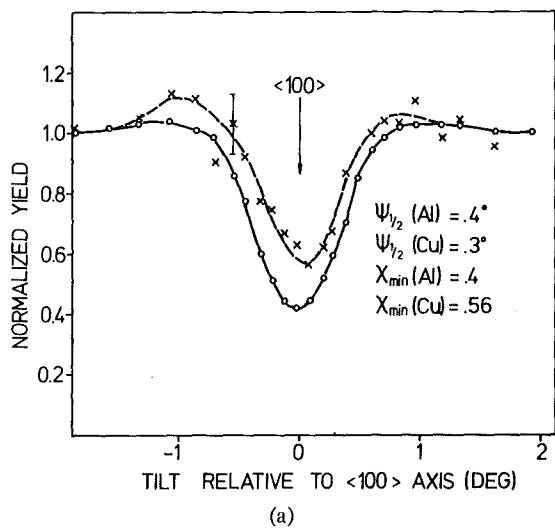
FIGURE 7 Angular scans of the backscattered ^{4}He yield from a Cu implanted aluminium crystal (relative to (a) $\langle 100 \rangle$ and (b) $\langle 110 \rangle$ as indicated). Cu (x———x) and Al (0———0). Incident beam of 2.0 MeV ^{4}He$^+$.

calculated by using the empirical formula of Barrett[23]

$$\Psi_{1/2} = 0.8 F_{RS}\left(\frac{1.2 u_1}{a}\right)\Psi_2$$

where

$$\Psi_2 = 0.307\left(\frac{Z_1 Z_2}{Ed}\right)^{1/2}$$

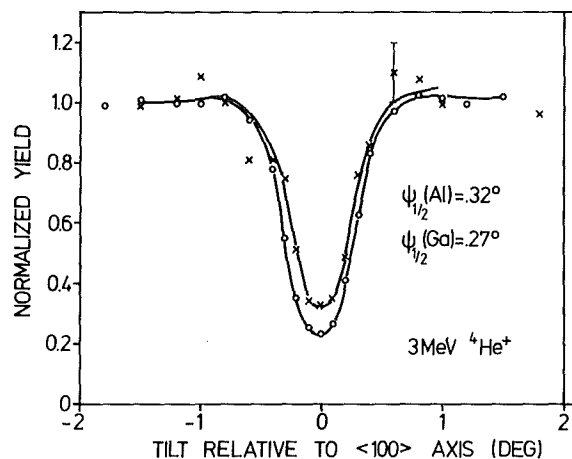degrees. Z_1 and Z_2 are the atomic numbers of He and Al respectively, d is the distance between

FIGURE 8 $\langle 100 \rangle$ angular scan of the backscattered ^{4}He yield from a Ga implanted Al crystal at 3.0 MeV ^{4}He$^+$. Ga (x — — — x) and Al (0———0).

adjacent Al atoms, a is the Thomas Fermi screening radius for Al and u_1 is the one dimensional rms vibrational amplitude.

Table II shows the experimental and calculated critical half angles along $\langle 100 \rangle$ for both impurities (Cu and Ga) and the host lattice at 3 different analyzing energies. The Debye temperatures θ_D used in the calculations to obtain an agreement with the experimental values are indicated in the table. For the host lattice a lower θ_D than the usual value of 390 K had to be inserted in the formula of u_1.[24] This procedure had to be adopted to obtain a realistic estimate of the displacements of the impurity atoms from the ideal lattice positions. These displacements were obtained from $\sqrt{u_i^2 - u_h^2}$, where u_i is the one dimensional rms thermal vibrational amplitude for the impurity and u_h is that for the host and are shown in the table. Good agreement for the calculated critical angles for the host lattice and for the impurity atoms has been obtained for the different analyzing energies.

SUMMARY AND CONCLUSIONS

S, Ca, Cu, Ga, Ge and Cs ions were implanted into aluminium single crystals with energies corresponding to similar projected ranges for the different ions. The lattice position of the implanted ions has been determined and the disorder in the aluminium host lattice has been analyzed by the

TABLE II

Experimental and calculated critical half angles for the host and impurities along the
$\langle 100 \rangle$ axis at 3 different energies and the average displacement of the impurity atoms

Impurities	Analyzing He$^+$ beam energy (MeV)	$\Psi_{1/2} \langle 100 \rangle$ (degrees)				Displacement $\sqrt{u_i^2 - u_h^2}$ (Å)
		Host		Impurity		
		Exp.	Cal.[a]	Exp.	Cal.[b]	
Cu	1	.525	.565	.422	.423	
	2	.402	.40	.3	.299	.198
	3	.32	.326	.235	.244	
Ga	1	.533	.57	.458	.467	
	2	.41	.405	.332	.33	.157
	3	.323	.33	.272	.27	

[a] For host, these values are calculated by considering the Debye temperature as 315 K
(for Cu implanted) and 330 K (for Ga implanted) which give the corresponding thermal
vibrational amplitudes .130 Å and .125 Å respectively.

[b] For impurities, these values are calculated by considering the Debye temperature
as 170 K (for Cu) and 200 K (for Ga), the corresponding thermal vibrational amplitudes
are .237 Å (for Cu) and .201 Å (for Ga).

investigation of the energy dependence of the de-
channelling cross-sections. These energy dependent
analyses showed the presence of different types of
defects depending on implanted ions species. In
the spectra of Cu, Ga, Ge and Cs implanted
samples an initial monotonous increase of the
dechannelling yield was observed with a "knee"
indicating the depth of the disorder. This disorder
depth is observed to be considerably larger than
the corresponding LSS ions range for these ions
(Table I). This behaviour shows the presence of
extended defects and shadows a direct backscatter-
ing component if present. The dechannelling cross-
section showed a linear dependence with $\sqrt{E}$
within the experimental errors for the ions indicated
above. According to the suggestions of Quéré this
dependence is consistent with the presence of
dislocations. Similar conclusions referring to the
nature of the damage have been drawn previously
for Zn implanted Al crystals and the presence of
dislocations in the samples has been shown directly
by complementary TEM analysis.[19,25] Though
the shape of the spectra and thus the nature of dis-
order were almost similar for the different ions,
differences arose in the slope of the dechannelling
yields vs depth and in their absolute values.

Rapid increases behind the surface peak and
high absolute values of the dechannelling yield
were observed for Cs and Cu indicating higher
dislocation densities if the dechannelling cross-
section is assumed to be constant as compared to

Ga and Ge where the dechannelling yield is
relatively lower and the increase vs. depth is not
very steep. This different behaviour does not
correlate with substitutional lattice site occupation
of the implanted ions as a similar behaviour in the
host lattice distortion was detected for ions showing
an opposite nature in the lattice site distribution.
Here further experiments are necessary with dis-
order studies as a function of impurity concentra-
tion. The reason for quantitatively different dis-
tortions may be due to the interaction of impurities
with defects which in turn may depend on a so far
unknown atomic species parameter like, e.g. atomic
size or electronegativity.

S and Ca ions showed a different influence on
the host lattice disorder as compared to Cu, Ga,
Ge and Cs. Here in the aligned backscattering
spectra a direct backscattering peak emerged at
high analyzing energies approximately within the
measured range distribution of the implanted ions.
Such a peak indicates largely displaced host lattice
atoms. Again an atomic arrangement like in a poly-
crystal could also give rise to a direct backscattering
peak. But the formation of polycrystals seems
improbable in these experiments. Backscattering
peaks in implanted Al crystals were observed pre-
viously with N ions by Rimini et al.[12] and explained
by intrinsic Al defects or the influence of N with
possible nitride precipitations.

Concerning the influence of defects on the super-
conducting transition temperature T_c in implanta-

tion experiments of different ions into aluminium layers the following conclusions can be drawn from the energy dependent defect analysis and lattice location studies in the present investigation:

A disordered host lattice with locally displaced atoms formed for S and Ca implantation correlates with a rather high increase of $T_c (\Delta T_c \geq 0.5$ K); ions occupying substitutional lattice positions like Cu and Ga and also detected in Zn implanted Al-sample[12] and Ag implanted Al-sample[25] cause smaller changes in $T_c (\Delta T_c \leq 0.2$ K) probably due to minor distortions of the host lattice; Cs, though causing a substantial increase of T_c, did not show a direct backscattering peak in the implanted crystals, however revealed a high degree of long range disorder. The high dechannelling component may overshadow the presence of locally displaced atoms, however also the high long range order defect concentration may correlate with the T_c increase. This possibility is supported by the comparison of the plots in Figure 3 where the energy dependence of the dechannelling cross section is plotted for ions causing mainly extended defects and at least a qualitative correlation is observed between defect concentration and T_c increase. Thus from the defect and lattice location studies in Al single crystals it may be concluded that the T_c increases are due to distortion of the Al host lattice rather than to alloying effects. Different degrees of disorder are stabilized with the different implantation conditions including especially the ion species.

REFERENCES

1. J. W. Mayer, L. Eriksson, and J. A. Davies, *Ion Implantation in Semiconductors*, Academic Press, New York and London (1970).
2. G. Linker, M. Gettings, and O. Meyer, *Ion Implantation in Semiconductors and Other Materials*, ed. B. L. Crowder; Plenum Press, New York and London (1973), p. 465.
3. P. P. Pronko, J. Bottiger, J. A. Davies, and J. B. Mitchell, *Rad. Eff.*, **21**, 25 (1974).
4. D. K. Sood and G. Dearnaley, *J. Vac. Sci. Techn.*, **12**, 445 (1975).
5. P. P. Pronko, *Nucl. Instr., Meth.*, **132**, 249 (1976).
6. Y. Quéré, *Rad. Eff.*, **28**, 253 (1976).
7. Y. Quéré, *Phys. Stat. Sol.*, **30**, 713 (1968).
8. D. Ronikier-Polonsky, G. Desarmot, N. Housseau and Y. Quéré, *Rad. Eff.*, **27**, 81 (1975).
9. J. C. Jousset, J. Mory, and J. J. Quillico, *J. Physique (Let.)*, **35**, L 229 (1974).
10. G. Linker, *Nucl. Instr. Meth.*, **149**, 365 (1978).
11. M. K. Agrawal and D. K. Sood, *Nucl. Instr. Meth.*, **149**, 425 (1978).
12. E. Rimini, S. U. Campisano, G. Foti, and P. Baeri, *Ion Beam Surface Layer Analysis*, eds. O. Meyer, G. Linker, and F. Käppeler, Plenum Press, New York and London (1976), p. 597.
13. A. Turos, L. Wieluński, M. Wieluński, and B. Wojtowicz-Natanson, *Nucl. Instr. Meth.*, **149**, 421 (1978).
14. S. U. Campisano, G. Foti, E. Rimini, and S. T. Picraux, *Nucl. Instr. Meth.*, **149**, 371 (1978).
15. O. Meyer, *Ion Implantation in Semiconductors*, ed. S. Namba, Plenum Press, New York and London (1975), p. 301.
16. T. Hussain and G. Linker, *Nucl. Instr. Meth.*, **168**, 317 (1980).
17. J. F. Ziegler and W. K. Chu, *Atomic Data and Nuclear Data Tables*, **14**, 436 (1974).
18. K. L. Merkle, P. P. Pronko, D. S. Gemmell, R. C. Mikkelson, and J. R. Wrobel, *Phys. Rev.*, **B8**, 1002 (1973).
19. G. Foti, S. T. Picraux, S. U. Campisano, E. Rimini, and R. A. Kant, *Ion Implantation in Semiconductors*, eds. F. Chernow, J. A. Borders, and D. K. Brice, Plenum Press, New York and London (1977), p. 247.
20. R. Kalish and L. C. Feldman, *Ion Implantation in Semiconductors*, eds. F. Chernow, J. A. Borders, and D. K. Brice, Plenum Press, New York and London (1977), p. 239.
21. M. L. Swanson and F. Maury, *Can. J. Phys.*, **53**, 1117 (1975).
22. J. L. Merz, L. C. Feldman, D. W. Mingay, and W. M. Augustyniak, *Ion Implantation in Semiconductors*, eds. I. Ruge and J. Graul, Springer-Verlag, Berlin (1971), p. 182.
23. J. H. Barrett, *Phys. Rev.*, **B3** 1527 (1971).
24. W. K. Chu, J. W. Mayer, and M. A. Nicolet, *Backscattering Spectrometry*, Academic Press, New York and London (1978), p. 236.
25. S. T. Picraux, E. Rimini, G. Foti, and S. U. Campisano, *Phys. Rev.*, **8B**, 2078 (1978).
26. D. K. Sood and G. Dearnaley, *Application of Ion Beams to Materials*, eds. G. Carter, J. S. Colligon, and W. A. Grant, Conference Series No. 28, The Institute of Physics, London and Bristol (1976), p. 196.

DEPENDENCE OF DEFECT STRUCTURES ON IMPLANTED IMPURITY SPECIES IN Al SINGLE CRYSTALS

T. HUSSAIN* and G. LINKER

Institut für Angewandte Kernphysik, Kernforschungszentrum Karlsruhe GmbH, P.O.B. 3640, D-7500 Karlsruhe, Germany

Aluminium single crystals have been implanted with Ca and Ga ions. Energy dependent channeling and backscattering experiments for disorder analysis together with lattice site determination have been performed with ^{4}He$^+$ ions in the energy range 1.0–3.0 MeV. A high substitutional fraction of 87% and disorder consisting mainly of extended defects (dislocations) has been detected for Ga implanted crystals. For Ca implanted samples local distortions of the Al host lattice and an interstitial distribution of the impurities have been observed. The different kinds of damage correlate with previously observed different changes of the superconducting transition temperature in ion implanted Al layers.

1. Introduction

Many properties of solids, in particular also the superconducting properties like the critical temperature, the critical field or the critical current are affected by the presence of impurity atoms and defects. Ion implantation is a method to introduce impurities into near surface regions of solids and to create defects by the energy transfer of the bombarding particles during nuclear collisions. In aluminium it is known that structural distortions will lead to an increase of the superconducting transition temperature T_c. Quantitatively different T_c increases depending on implanted ion species have been observed in implantation experiments into evaporated aluminium thin films[1]. Layers implanted with N, S, Ca or Cs ions showed a rather high T_c increase ($\Delta T_c \geq 0.5$ K) while a small or no effect was observed for Cu, Zn, Ga and Ag ($\Delta T_c \leq 0.2$ K). The different influences on T_c were ascribed to qualitatively different defect structures.

For a better understanding of these findings results are presented in this paper on defect and lattice location studies for two representative ions namely Ca and Ga implanted into aluminium single crystals. Channeling and backscattering measurements with He ions were performed for the analysis. Though the defect structure of ion bombarded metals has not been as widely studied as in the case of semiconductors, the channeling technique is a convenient tool for, at least qualitative, disorder characterization in metals. Here instead of a disorder peak (which is usually observed in ion

implanted semiconductors) generally a monotonous increase of the dechanneling yield with depth is observed indicating the presence of extended defects like dislocations, interstitial clusters, grain boundaries with associated strains etc. The disorder region in many cases extends to depths much deeper than the ions projected range. According to the suggestions of Quéré[2]) the energy dependence of the dechanneling cross sections may allow to determine the presence of different kinds of defects. Therefore energy dependent channeling measurements have been performed together with lattice location determination in order to test if a correlation exists between lattice site distribution of the impurity atoms and defect structure, and whether different defects correlate with previously observed changes of T_c. The hypothesis that these changes were due to distortions of the Al host lattice rather than to alloying was also tested.

2. Experimental

Single crystal aluminium slices of ⟨100⟩ orientation were used for the channeling and backscattering experiments. The samples were implanted with 90 keV Ca$^+$ ions with fluences of 6.5×10^{15} ions/cm^2 and 1.5×10^{16} ions/cm^2 and with 150 keV Ga$^+$ ions with a fluence of 5.3×10^{15} ions/cm^2. These implantation energies correspond to LSS projected ranges of 72 nm and 78 nm for Ca and Ga, respectively. All implantations were performed at room temperature and along random directions. The analyses of the implanted samples were done with a well collimated ^{4}He$^+$ beam in the energy range 1–3 MeV obtained from a Van de Graaff accelerator. Alignment of the crystals and angular scans

were performed with the help of an electronically controlled three-axis goniometer with an adjusting accuracy of 0.01°. Particles backscattered at an angle of 165° were detected by a solid state surface barrier detector with an energy resolution of 15 keV. The samples were rotated around an axis well of the channeling direction for detection of the random spectra.

3. Results

3.1. GA IMPLANTATION

In fig. 1, ⟨100⟩ aligned backscattering spectra of a Ga implanted crystal are shown at analyzing beam energies of 1.0, 1.5, 2.0 and 3.0 MeV. The spectra reveal a linear increase of the dechanneling yield as a function of depth. No change of the shape of the spectra has been observed with increasing beam energy.

The average dechanneling defect cross section can be determined according to the method of Merkle et al.[3]) using the formula

$$\sigma_d = \frac{1}{N_s} \Delta \left(\frac{\delta \chi}{\delta z} \right) \frac{1}{1 - \chi_{min}} \tag{1}$$

developed for dechanneling from defect clusters.

Here N_s is the defect density, $\Delta(\delta x/\delta Z)$ is the damage induced change of the dechanneling rate and χ_{min} is the minimum yield. The value of $\sigma_d N_s$
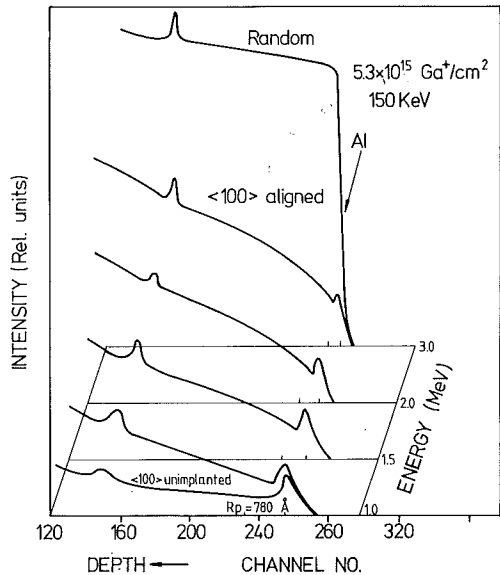
in this experiment was obtained from the slope of the line fitting the data points in the spectra in the region of maximum disorder. This procedure has been adopted because of the low increase of the dechanneling yield in the unimplanted crystals. The minimum yield was determined by extrapolation of the lines to the surface. Using eq. (1) the product $\sigma_d N_s$ has been determined for the different analyzing beam energies. The results are shown in fig. 2 where $\sigma_d N_s$ is plotted as a function of $\sqrt{E}$. The figure shows the variation of σ_d with the beam energy directly since N_s is independent of energy for a particular sample. A straight line passing through the experimental points suggests a $\sqrt{E}$ dependence of the dechanneling cross section.

For the lattice position determination of the implanted Ga ions angular scans were performed and from the data the substitutional fraction f_s has been calculated using the formula[4]):

$$f_s = (1 - \chi_i)/(1 - \chi_h),$$

where χ_i is the normalized minimum yield from the impurity and χ_h that for the host at the position of the implanted ions. Since in crystals with fcc structure a 17% shadowing for atoms significantly displaced (0.05–0.15 nm) into the ⟨110⟩ direction occurs when channeling experiments are performed into ⟨110⟩ direction[5]), additional angular scans were performed along the ⟨100⟩ direction to obtain an unambiguous lattice site determination.

Figs. 3a and 3b show the angular scans of the backscattered $^4He^+$ ion yield across the ⟨100⟩ and ⟨110⟩ channels at an incident beam energy of 2 MeV. The substitutional fractions determined from both channeling directions were found to agree within the experimental error. A substitutional fraction of about 87% has been found for Ga in
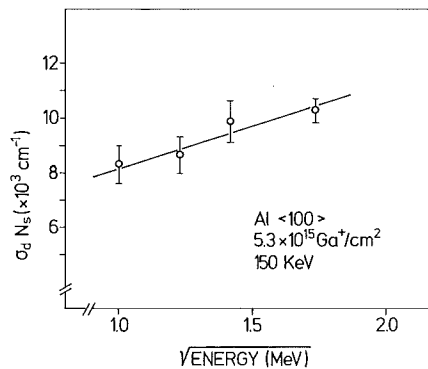

Fig. 1. Backscattering spectra of a ⟨100⟩ aligned Al crystal implanted with 5.3×10^{15} Ga$^+$/cm^2, 150 keV, at four different analyzing beam energies. A random and an aligned spectrum for an unimplanted crystal are also shown. Different depth scales in the spectra are indicated by the ions projected range R_p.

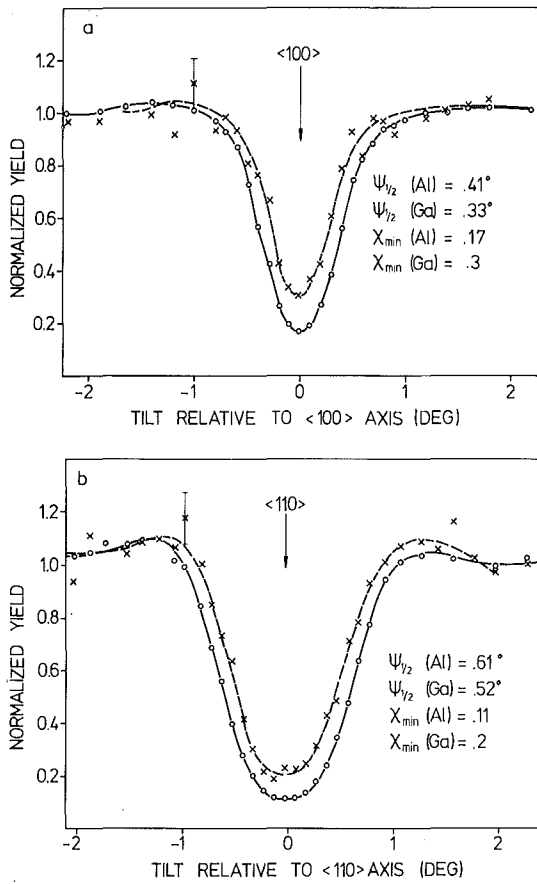Fig. 2. Dependence of $\sigma_d N_s$ on the square root of the analyzing beam energies of a ⟨100⟩ aligned Al crystal implanted with Ga$^+$.

Fig. 3. Angular scan of the backscattered $^4He^+$ yield from a Ga$^+$ implanted aluminium crystal (relative to (a) $\langle 100 \rangle$ and (b) $\langle 110 \rangle$ as indicated). Ga (crosses) and Al (circles). Incident beam of 2.0 MeV $^4He^+$.

Al. However, the narrowing of the angular width for the impurity atoms as compared to the scan from the host lattice indicates slight displacements of the impurity atoms from the ideal lattice position. A value of about 0.016 nm for the $\langle 100 \rangle$ direction has been estimated for this displacement using Barrett's formula[6]).

3.2. Ca implantation

Samples implanted with Ca ions were analyzed with a $^4He^+$ beam of 1.0, 2.0 and 3.0 MeV. The aligned and random spectra at these energies are shown in figs. 4a and 4b. In the spectra at 1 MeV analyzing energy a monotonous increment of the dechanneling yield behind the surface peak can be observed. At higher energies however a well resolved disorder peak appears in the spectra approximately within the measured range distribution of the implanted Ca ions. With the introduc-

tion of higher doses the disorder peak becomes more prominent as can be noticed from the fig. 4b indicating the presence of larger disorder. Due to the appearance of a disorder peak here a different procedure for the analysis of the energy dependence of the dechanneling yield has been used. The dechanneling yield $\Delta\chi$ has been determined as the difference of the normalized yields of the implanted and the unimplanted samples at a depth behind the disorder peak (about 220 nm). The results are plotted in fig. 5 as a function of the beam energy. Here
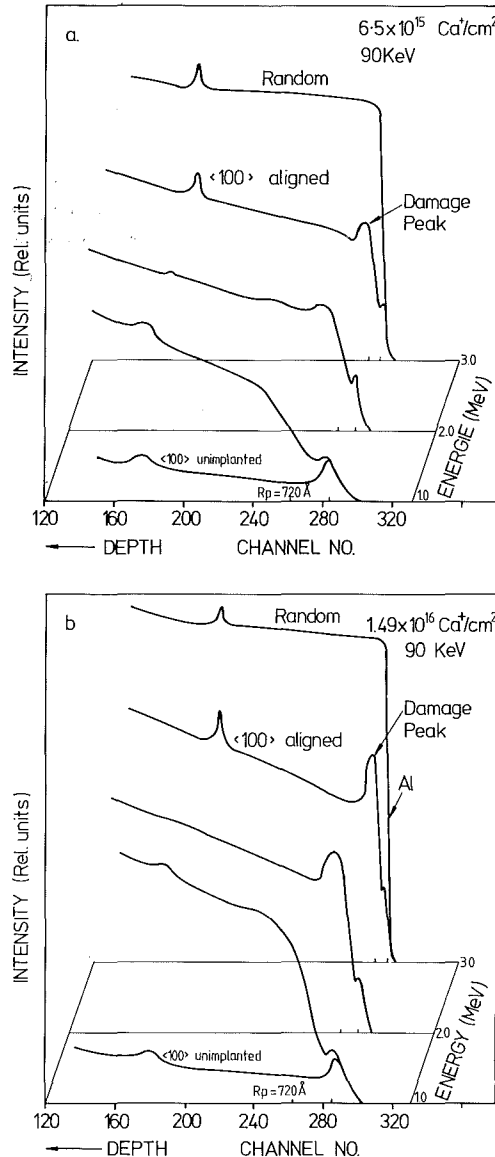

Fig. 4. Backscattering spectra at three different beam energies from $\langle 100 \rangle$ aligned Al crystals implanted with (a) 6.5×10^{15} Ca$^+$/cm^2, 90 keV; (b) 1.5×10^{16} Ca$^+$/cm^2, 90 keV.
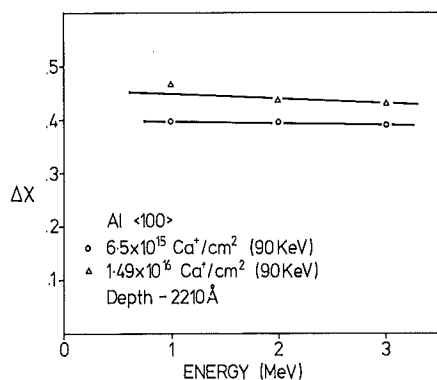
Fig. 5. Dechanneling yield $\Delta\chi$ from Ca^+ implanted Al crystals as a function of the analyzing beam energies. $\Delta\chi$ was determined at a depth of 2210 Å (behind the damage peak).

a slight decrease of $\Delta\chi$ with increasing energy is observed in accordance with that part of disorder which gives rise to a direct backscattering peak. Such a peak indicates largely displaced lattice atoms in the host lattice. It should be noticed however that this statement is not unique because, e.g., an atomic arrangement like in a polycrystal would also give rise to a direct backscattering peak. The formation of polycrystals however seems improbable in these implantation experiments. Similar types of results have been observed previously in nitrogen implanted vanadium and carbon implanted molybdenum single crystals[7]. From the high intersection value of the straight line fitted through the experimental points on the $\Delta\chi$ axis one can conclude that the main portion of the dechanneling arises from other defects probably having an energy independent dechanneling cross section.
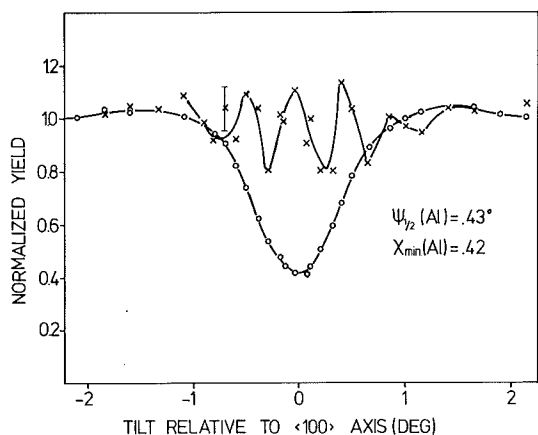

Fig. 6. Angular scan of the backscattered $^4He^+$ yields from a Ca^+ implanted $(6.5\times10^{15}$ $Ca^+/cm^2)$ Al-crystal (relative to $\langle100\rangle$ axis). Ca (crosses) and Al (circles). Incident beam of 2.0 MeV $^4He^+$.

Almost no substitutional lattice position has been observed from Ca yields determined in the $\langle100\rangle$ aligned and random spectra. However, the angular scan across the $\langle100\rangle$ axis showed (fig. 6) oscillations in the Ca yield indicating the presence of different interstitial positions. Different interstitial sites for light atoms in metals have been observed previously with channeling measurements e.g. for D and ^3He in W^8), and also the appearance of distinct interstitial sites for large ions (Br in Fe) has been already reported[9].

4. Summary and conclusions

Ca and Ga ions were implanted into aluminium single crystals with energies corresponding to similar projected ranges. These ions were known to produce different changes of the superconducting transition temperature in implanted Al layers. The energy dependent analysis showed the presence of different kinds of defects depending on the implanted ion species. For the Ga implanted sample the linear increase of the dechanneling cross section with $\sqrt{E}$ indicates that disorder consists mainly of extended defects which could shadow a direct backscattering component if present. According to the suggestions of Quéré a linear relationship between σ_d and $\sqrt{E}$ shows the existence of dislocations. Similar conclusions referring to the nature of disorder have been drawn previously for Zn implanted Al crystals and the presence of dislocations in the samples has been shown directly by complementary TEM analysis[10].

Ca ions had a different influence on the host lattice disorder. Here a disorder peak with the peak area growing with the implanted dose, demonstrates the presence of local scattering centres, whose arrangement in the lattice however was not determined in the present measurements. Also the high dechanneling component behind the disorder peak demonstrates that other types of defects were also produced by the implantation. It is difficult to determine the nature of this disorder unambiguously by channeling measurements only, as the true energy dependence may be obscured by the presence of more than one kind of defects having energy dependences opposite in nature.

Disorder peaks in implanted Al crystals were observed previously with nitrogen ions and explained by intrinsic aluminium defects or possible nitride precipitation[11]. Here it is believed that the local displacements of the host lattice atoms are connected with an interstitial lattice site distribution

of the Ca atoms which was indicated in the angular scan measurements. An interstitial lattice position for an atom with big atomic radius like Ca probably is possible only in a locally disturbed host lattice.

Concerning the influence of defects on the superconducting transition temperature in implantation experiments, the following conclusions can be drawn from the defect analysis and lattice location study in this investigation: a disordered host lattice with locally displaced atoms found for Ca implantations correlates with the observed rather high T_c increase. Ions occupying substitutional lattice positions like Ga cause smaller changes of T_c probably due to the observed minor distortions of the host lattice consisting mainly of extended defects. Thus, the hypothesis from the implanted layer results that the T_c increases are due to local distortions of the Al host lattice rather than to alloying has been substantiated. Different degrees of disorder are stabilized under different implantation conditions and depend especially on the implanted ion species.

References

[1] O. Meyer, J. Jap. Soc. Appl. Phys. **44** (1975) 23.

[2] Y. Quéré, Rad. Effects **28** (1976) 253.

[3] K. L. Merkle, P. P. Pronko, D. S. Gemmell, R. C. Mikkelson and J. R. Wrobel, Phys. Rev. **B8** (1973) 1002.

[4] J. L. Merz, L. C. Feldman, D. W. Mingay and W. M. Augustyniak, in Ion implantation in semiconductors, eds. I. Ruge and J. Graul (Springer-Verlag, Berlin, 1971) p. 182.

[5] M. L. Swanson and F. Maury, Can. J. Phys. **53** (1975) 1117.

[6] J. H. Barrett, Phys. Rev. **B3** (1971) 1527.

[7] G. Linker, Nucl. Instr. and Meth. **149** (1978) 365.

[8] S. T. Picraux and F. L. Vook, in Application of ion beams to metals, eds. S. T. Picraux, E. P. EerNisse and F. L. Vook (Plenum Press, New York and London, 1973) p. 407.

[9] R. B. Alexander, P. T. Callaghan and J. M. Poate, Phys. Rev. **B9** (1974) 3022.

[10] G. Foti, S. T. Picraux, S. U. Campisano, E. Rimini and R. A. Kant, Ion implantation in semiconductors, eds. F. Chernow, J. A. Borders and D. K. Brice (Plenum Press, New York and London, 1977) p. 247.

[11] E. Rimini, S. U. Campisano, G. Foti and P. Baeri in Ion beam surface layer analysis, eds. O. Meyer, G. Linker and F. Käppeler (Plenum Press, New York and London, 1976) p. 597.

Improvement of lattice site location of Ga implanted into Al after pulsed electron beam annealing

T. Hussain, [a] J. Geerk, F. Ratzel, and G. Linker

Institut für Angewandte Kernphysik, Kernforschungszentrum Karlsruhe GmbH, Box 3640, D-7500 Karlsruhe, Federal Republic of Germany

The effect of pulsed electron beam annealing (PEBA) on the lattice location and impurity distribution of Ga ions implanted into Al single crystals has been compared with the thermal annealing behavior of this ion/target system. While with thermal annealing only slight improvement of the lattice site occupation was observed after PEBA within experimental accuracy, all implanted impurities occupied perfect lattice sites. In the thermal treatment the Ga atoms partially diffused out of the implanted region; with PEBA, however, the implanted impurity distribution remained unchanged.

PACS numbers: 81.40.Ef

There is growing interest in the development of non-equilibrium techniques for the production of metastable compounds and supersaturated solid solutions. Splat cooling and ion implantation, e.g., have been used to exceed thermal solubility limits. In addition, recently pulsed beam heating has been employed successfully to study the annealing behavior of implanted-ion/target systems. While most of the work has been performed with pulsed laser beams on implanted semiconductors, only a few attempts have been made to anneal metallic systems.[1] This is probably due to the difficulties of coupling lasers to polished metallic surfaces with high reflectivity. In metals, pulsed electron beams[2] are expected to be a convenient method for transient annealing of implanted surface regions.

In this letter, results from pulsed electron beam annealing (PEBA) are compared with those from thermal treatment of Al single-crystal samples implanted with Ga ions. In previous experiments it had been found that, although Ga ions implanted into Al single crystals occupied substitutional lattice positions to a high fraction, they were displaced on the average to about 0.16 Å from the ideal lattice sites.[3] It was therefore of interest to study whether an improvement of the lattice site distribution could be achieved with different annealing techniques.

Aluminum single crystals have been implanted with 7×10^{15} Ga$^+$/cm^2 at 150 keV, corresponding to a concentration of about 1 at. %. The depth distribution of the implanted ions and their lattice location have been studied before and after annealing using Rutherford backscattering and channeling effect measurements with 2-MeV ^{4}He$^+$ ions. The thermal treatment has been performed in a vacuum furnace at temperatures of 100, 200, 250, 300, and 350 °C
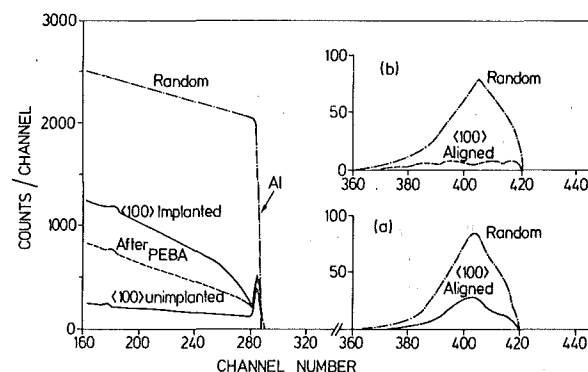

FIG. 1. Random and ⟨100⟩ aligned backscattering spectra of an Al single crystal implanted with 7×10^{15} Ga$^+$/cm^2 at 150 keV before and after pulsed electron beam annealing. The parts of the spectra on the right side of the figure reflect the Ga distribution before (a) and after (b) PEBA.

---

[a]On leave from Physics Dept., Univ. of Dacca, Bangladesh.

and heating times of 1 h. Pulsed electron beams have been obtained from a system whose operation is described elsewhere.[4] Electron beams with maximum energies of about 15 keV and pulse duration of 300 nsec have been used in those experiments. The annealing behavior has been studied as a function of the deposited energy. The samples have been exposed successively to four single pulses of 0.6 J/cm^2.

Figure 1 shows random and aligned backscattering spectra from the as-implanted Al crystal and after PEBA treatment with a total deposited energy of 2.4 J/cm^2. In the right part of the figure the Ga distributions before 1(a) and after 1(b) annealing are shown. While in the random distribution of the impurity atoms little change is observed after annealing, in the $\langle 100 \rangle$ aligned spectra the yield from the Ga atoms is considerably reduced. This reduction indicates that some of the Ga atoms which initially were not on substitu-
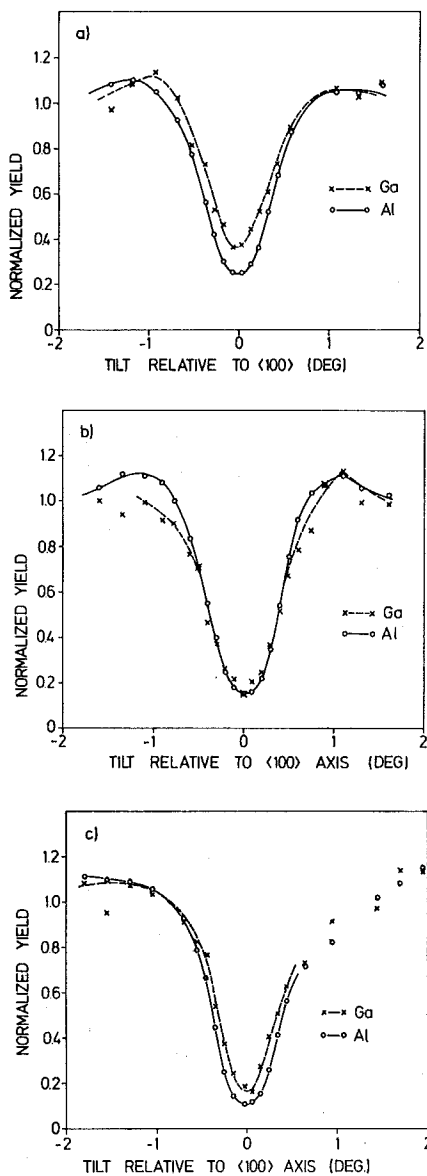
tional sites moved to substitutional lattice positions. The reduction of the dechanneling yield in the part of the spectrum arising from backscattering from the Al atoms (left part of the figure) indicates some, though not complete annealing of the host lattice.

In Fig. 2 angular scan measurements from the host and the impurity atoms along the $\langle 100 \rangle$ axis are shown before annealing (a), after PEBA (b), and after thermal annealing (c). Analysis of the angular yield curves from the as-implanted crystals showed that about 85% of the Ga atoms occupied substitutional sites as calculated from the formula
$f_s = (1 - \chi_i)/(1 - \chi_h)$, where f_s is the substitutional fraction and χ_i and χ_h are the normalized minimum yields for the impurities and the host lattices. The narrowing of the yield curve from the impurities indicates that the Ga atoms are displaced from the ideal lattice sites on the average by about 0.16 Å. These results are in accordance with earlier experiments[3] where angular scan measurements were performed in both $\langle 100 \rangle$ and $\langle 110 \rangle$ directions.

In the pulsed electron beam annealing process a continuous improvement of the agreement of the angular yield curves from the host lattice and the impurity atoms was observed, with the shape of the yield curve from the impurities approaching that from the host, whose width remained unchanged. The best result after annealing with a total deposited energy of 2.4 J/cm^2 is demonstrated in Fig. 2(b). Though no complete agreement was obtained in the overall shape of the curves, the χ_{min} values and the $\psi_{1/2}$ values (half width at half height) were identical, showing that almost all Ga atoms were now on perfect substitutional sites.

With thermal annealing an improvement of lattice site occupation was also observed. The best result was obtained in the temperature range 250–300 °C, where it was observed that about 93% of the Ga atoms occupied substitutional sites. However, here, as shown in Fig. 2(c) a narrowing of the yield curve from the impurities still remained, i.e., the Ga atoms were slightly displaced from the perfect lattice position. The annealing behavior of the host lattice in the thermal treatment was similar to that observed after PEBA.

In addition, in the thermal treatment a redistribution of the implanted impurities was observed. This behavior is illustrated in Fig. 3, where random and aligned backscattering
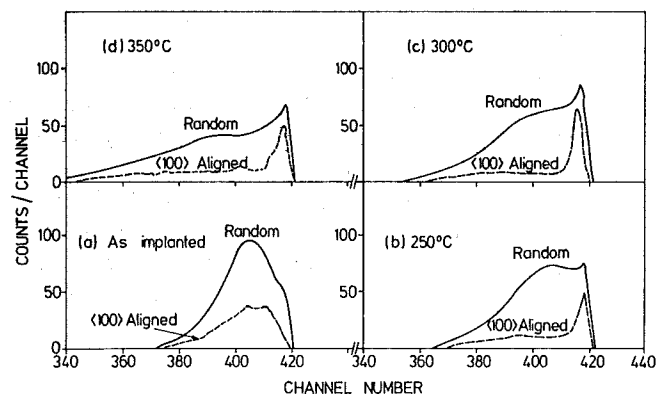

FIG. 2. Angular scan measurements for Ga and Al along the $\langle 100 \rangle$ direction for the as-implanted sample (a), after PEBA with 2.4 J/cm^2 (b), and after thermal treatment at 250 °C (c).

FIG. 3. Backscattering spectra from Ga atoms showing the distribution of the impurities in the thermal annealing process at different temperatures.

299   Appl. Phys. Lett., Vol. 37, No. 3, 1 August 1980

Hussain *et al.*   299

spectra reflect the depth distribution of the Ga atoms in an isochronal annealing treatment. These distributions should be compared to those shown in Fig. 1(a) and in 1(b) after PEBA treatment. Some impurity segregation at the crystal surface can be observed in the aligned spectra, and diffusion into the bulk out of the implanted region is also clearly demonstrated.

In conclusion, the comparison of thermal with pulsed electron beam annealing revealed two principle advantages of PEBA over the conventional thermal method in the Ga-Al implantation system: (i) With PEBA, in contrast to thermal annealing, the implanted impurity distribution did not change. This is a promising result with respect to the production of metastable alloys with higher impurity concentrations. (ii) With PEBA the improvement of lattice site occupation was much more effective than with thermal annealing.

With the electrons penetrating to a depth of about 1.5 μm, the average temperature rise in the regime of annealing was estimated to be ~ 350 °C, which is well below the melting point of aluminum and comparable to the highest temperature applied in the thermal treatment. Thus it is thought that both advantages of PEBA are due to the fast cooling rate achieved with this method. The cooling rate for transient annealing in Si has been estimated to be about 10^9 K/sec,[5] and for Al one can expect even higher cooling rates because of the better heat conductivity of this material.

[1]Proceedings, *Laser Effects in Ion Implanted Semiconductors*, Catania, 1978, edited by E. Rimini (University of Catania, Catania, 1979).
[2]A. R. Kirkpatrick, R. G. Little, A. C. Greenwald, and J. A. Minnucci, in Ref. 1, p. 232.
[3]T. Hussain and G. Linker, Nucl. Instrum. Methods **168**, 317 (1980).
[4]J. Geerk and F. Ratzel, KfK Report No. 2912 (unpublished, 1979).
[5]A. C. Greenwald, A. R. Kirkpatrick, R. G. Little, and J. A. Minnucci, J. Appl. Phys. **50**, 783 (1979).